JOURNAL OF THERMOPHYSICS AND HEAT TRANSFER
Vol. 6, No. 2, April–June 1992

Modeling of an Argon Plasma in a Boundary-Layer Flow

Pascale Domingo,* Dany Vandromme,† and P. Vervisch‡
CORIA—URA, 76134 Mont Saint Aignan, France

Results of the modeling of an argon plasma are compared against experiments in a laminar boundary-layer flow. The test conditions are as follows: pressure = 120 Pa, strong thermal nonequilibrium ($T_{\text{atom-ion}} \sim 1500$ K, $T_{\text{electrons}} \sim 5500$ K), ionization close to 1%. Ionization coefficient, population density of the $3p^54s$ level, velocity, and translational temperature are computed. The treatment of the $3p^54s$ level is performed including the radiative source terms. The numerical method used is a modified version of the Patankar and Spalding method. Comparison with experiments is fairly satisfactory. The influence of radiative transfer on the ion/electron recombination term is pointed out.

Nomenclature

C_p	=	specific heat coefficient for constant pressure
D_{amb}	=	ambipolar diffusion coefficient
D_m	=	diffusion coefficient for species $3p^54s$
(dN_e/dt)	=	ion/electron recombination coefficient
E_i^0	=	specific ionization energy
h_i	=	specific enthalpy for species i
N_i	=	number of particles of species i per volume unit
p_i	=	partial pressure
Q_{T-E}	=	energy exchanged by collision between heavy particles and electrons
q_i	=	heat flux of species i
r	=	perfect gas constant divided by the molar mass of argon (R/M_{Ar})
T	=	heavy particle temperature
u	=	x component of velocity
v	=	y component of velocity
α	=	mass fraction of argon ions
δ	=	boundary layer thickness
λ	=	thermal conductivity of species i
μ	=	dynamic viscosity
ρ	=	density
ρ_i	=	density for species i
Ψ	=	viscous dissipation function
$\dot{\omega}_i$	=	production rate of species i
$\langle\sigma\cdot v\rangle_{3p^54s\to 3p^54p}$	=	collision cross section

I. Introduction

FEW experimental investigations have been performed on plasmas in boundary-layer flows despite their great interest. Most works, such as those of Matsuoka and Nishida,[1] do not provide detailed information on the population of excited levels that are essential for the radiation prediction.

In this study, the results of the numerical calculations of a plasma boundary-layer flow are compared with experimental results. Prediction is needed for velocity, atomic temperature, mass fraction of argon ions, and population density at the $3p^54s$ level. A detailed radiative conservation equation, which prevents the use of effective transition probabilities is solved for the treatment of the $3p^54s$ level.

Received May 10, 1990; revision received Jan. 26, 1990; accepted for publication Feb. 5, 1990.

*Student, CFD Lab., CNRS 230 BP 118, INSA of Rowen.
†Professor, CFD Lab., CNRS 230 BP 118, INSA of Rowen. Member AIAA.
‡Senior Scientist, ThermoDynamic Lab., CNRS 230 BP 118, University of Rowen.

II. Mathematical Model

Governing equations are written with the classical boundary-layer assumption. The mode of the charged species diffusion is assumed to be ambipolar. Therefore, a unique equation is sufficient to describe the electron/ion pair evolution. The solid wall is assumed to be collision-free (sheath) and fully catalytic (total recombination). The transport equation for the $3p^54s$ level population corresponding to the resonant radiation transfer is included. Furthermore, the electron temperature is assumed to be constant in the boundary layer. This is verified experimentally. Indeed, electron temperature corresponds to a boundary-layer thickness about 10 times larger than the classical boundary-layer thickness δ inferred from the velocity profiles. As the calculation domain is scaled to δ, constant electron temperature is a reasonable approximation.

Transport equations for properties of the plasma are shown below.

A. Continuity Equation

$$\frac{\partial \rho u}{\partial x} + \frac{\partial \rho v}{\partial y} = 0 \tag{1}$$

B. Electron/Ion Pair Conservation Equation

$$\rho u \frac{\partial \alpha}{\partial x} + \rho v \frac{\partial \alpha}{\partial y} = \frac{\partial}{\partial y}\left(\rho D_{\text{amb}} \frac{\partial \alpha}{\partial y}\right) + \dot{\omega}_{Ar+} \tag{2}$$

with α being the ion mass fraction, D_{amb} the ambipolar diffusion coefficient, and $\dot{\omega}_{Ar+}$ the recombination rate of the charged species.

C. $3p^45s$ Level Population Conservation Equation

This level is made up of four components: two resonant levels and two metastable levels. Because of a high electron density the collisional coupling between these levels is strong and an overall description of the whole level can take the following form:

$$\rho u \frac{\partial}{\partial x} Y_{3p^54s} + \rho v \frac{\partial}{\partial y} Y_{3p^54s} = \frac{\partial}{\partial y}\left(\rho D_m \frac{\partial}{\partial y} Y_{3p^54s}\right) + \dot{\omega}_{3p^54s} \tag{3}$$

with Y_{3p^54s} the mass fraction, D_m the diffusion coefficient for the metastable and $\dot{\omega}_{3p^54s}$ its production rate.

D. Momentum Equation

$$\rho u \frac{\partial u}{\partial x} + \rho v \frac{\partial u}{\partial y} = -\frac{\partial p}{\partial x} + \frac{\partial}{\partial y}\left[\mu\left(\frac{\partial u}{\partial y}\right)\right] \tag{4}$$

E. Heavy Particle Energy Conservation Equation

$$u\frac{\partial}{\partial x}(\rho_{Ar^+}h_{Ar^+} + \rho_{Ar}h_{Ar}) + v\frac{\partial}{\partial y}(\rho_{Ar^+}h_{Ar^+} + \rho_{Ar}h_{Ar})$$
$$+ (\rho_{Ar^+}h_{Ar^+} + \rho_{Ar}h_{Ar})\left(\frac{\partial u}{\partial x} + \frac{\partial v}{\partial y}\right) + \frac{\partial}{\partial y}(q_{Ar^+} + q_{Ar})$$
$$-u\frac{\partial}{\partial x}(p_{Ar^+} + p_{Ar}) - v\frac{\partial}{\partial y}(p_{Ar^+} + p_{Ar})$$
$$-\frac{\rho}{\rho_{Ar^+}} D_{\text{amb}} \frac{\partial \alpha}{\partial y}\frac{\partial p_e}{\partial y} + \Psi = Q_{T-E} \tag{5}$$

Definition of the enthalpy variables gives:

$$\rho_{Ar^+}h_{Ar^+} + \rho_{Ar}h_{Ar} = \rho C_p T + \rho_{Ar^+}E_i^0 \tag{6}$$

Generalization of the Fourier heat flux law gives:

$$q_{Ar^+} + q_{Ar} = -(\lambda_{Ar^+} + \lambda_{Ar})\frac{\partial T}{\partial y}$$
$$+ (\rho_{Ar^+}V_{Ar^+} + \rho_{Ar}V_{Ar})C_p T \tag{7}$$

with λ_i being the thermal conductivity coefficient for species i and V_i being the diffusion velocity. Because of mass conservation the following relationship must be satisfied:

$$\rho_{Ar^+}V_{Ar^+} + \rho_{Ar}V_{Ar} = 0 \tag{8}$$

Radiative flux gives no contribution to this energy equation. Indeed, the inelastic collisions involving electrons are the more important, thus only free electron energy is affected by radiative term.

F. Transport Coefficients

1. Diffusion Coefficient for Ions

$$D_{\text{amb}} = D_{ia}[1 + (T_e/T)] \tag{9}$$

with T_e being the electron temperature and D_{ia} the diffusion coefficient for binary exchange between ions and atoms.[2]

The evolution of D_{ia} as a function of temperature as given by De Voto[3] leads to a significant difference between computations and experiments. Such a discrepancy results from the crude assumptions used for the evaluation of the ambipolar diffusion coefficient, which are not valid in strong thermal nonequilibrium situations. The following results have been obtained by taking an experimental diffusion coefficient, deduced from the integration of a transport equation. This technique is equivalent to using D_{ia} values three times larger than those in the literature. Furthermore, the difference cannot be attributed to the source terms because the chemistry is frozen for the charged particles in the boundary layer.

2. Diffusion Coefficient for Metastable Particles

This coefficient has been determined experimentally in postdischarge flows at 300 K (Refs. 4–6) and a power of 7/4 with temperature is assumed.

3. Thermal Conductivity[7]

$$\lambda_j = \frac{75}{16}k^2\frac{N_j T_j}{m_j}\left(\sum_i N_i\sigma_{ij}\left(\frac{8kT_j}{\pi m_j} + \frac{8kT_i}{\pi m_i}\right)^{1/2}\frac{2m_{ij}}{m_i}\right)^{-1} \tag{10}$$

where subscript j stand for species (Ar^+ or Ar) and: i = ions, atoms or electrons; N_i = number of particles of i species per volume unit; T_i = temperature of i species; σ_{ij} = effective collision section; k = Boltzman constant; and m_{ij} = reduced mass $m_{ij} = m_i m_j/(m_i + m_j)$ with m_i atomic mass of i species.

4. Viscosity

Mixture viscosity can be taken equal to argon viscosity with a Sutherland-type law.

5. Energy Transfer Between Heavy Particles and Electrons[8]

$$Q_{T-E} = 12\sqrt{2N_{Ar^+}^2}\left(\frac{m_e k T_e}{\pi}\right)^{1/2}\frac{k(T-T_e)}{m_{Ar^+}}$$
$$\cdot \sigma_{e-Ar^+}\left(1 + \frac{N_{Ar}\sigma_{e-Ar}}{N_{Ar^+}\sigma_{e-Ar^+}}\right) \tag{11}$$

III. Production Rates

A. Recombination Rate

As mentioned above, the chemistry is frozen for recombination in the boundary layer. Therefore, the crude relationship given by Hinnov and Hirschberg[9] is acceptable:

$$\dot{\omega}_{Ar^+} = m_{Ar}\left(\frac{dN_e}{dt}\right) \tag{12a}$$

with the ion/electron recombination coefficient:

$$\left(\frac{dN_e}{dt}\right) = \frac{1.16 \times 10^{-20} N_e}{T_e^{4.5}} \tag{12b}$$

B. Production Rate for Level $3p^54s$ Population

The kinetic scheme and simplifications are as follows:

$$Ar(s_j) + e^- \rightarrow Ar(1s^0) + e^- \tag{13a}$$
$$Ar^* \rightarrow Ar(s_j) + h\nu \tag{13b}$$
$$Ar(s_j) + e^- \rightleftharpoons Ar(si) + e^- \tag{13c}$$
$$Ar(s_j) + e^- \rightarrow Ar(pr) + e^- \tag{13d}$$
$$Ar(pr) \rightarrow Ar(s_i) + h\nu \tag{13e}$$
$$Ar^+ + 2e^- \rightarrow Ar(s_j) + e^- \tag{13f}$$
$$Ar(s_j) + Ar(si) \rightarrow Ar(1s^0) + Ar^+ + e^- \tag{13g}$$
$$Ar_{\text{res}}(s_j) \rightarrow Ar(1s^0) + h\nu \tag{13h}$$

with: $Ar(1s^0)$ = fundamental level; $Ar(s_j)$ = levels $3p^54s$ ($^1p_1$, $^3p_0$, $^3p_1$, $^3p_2$); $Ar(pr)$: levels $3p^54p$; Ar^* = excited levels other than $4p$ or $4s$; and $Ar_{\text{res}}(s_j)$: resonant levels of $3p^54s$ level.

The plasma studied here is of the recombination type. Saha equilibrium with excited level continuum is verified from the $3p^54p$ level up to the ionization limit. The $3p^54s$ level is overpopulated by a factor of 10 with respect to the equilibrium situation. The contribution of levels higher than $4p$ is neglected [reaction (13b)].

The high level of the electron density in the freestream ($\sim 7 \times 10^{+19}$) leads to a strong coupling between $3p^54s$ levels [reaction (13c)]. Thus, some equilibrium exists between these levels at the electron temperature. Experiments[10,11] show that these four levels follow the same evolution within the boundary layer.

Direct recombination on $4s$ levels [reaction (13f)] contributes little to the overall process, and therefore will be neglected. Reaction (13g), which is important only at low electron density, is also neglected. Therefore, only reactions (13a), (13d), (13e), and (13h) are considered.

The reaction rate (13a) is determined by microreversibility using data from Lloyd et al.,[12] Borst,[13] and Brunt et al.[14]

Reaction (13e), corresponding to the radiative transition of higher levels, has the following production rate:

$$\left(\frac{dN_{3p^54s}}{dt}\right)_{13e} = \sum_{4p\,\text{levels}} N_{3p^54p} A_{4p\to 4s} \tag{14}$$

$3p^54p$ level populations are calculated from a Saha distribution and the transition probabilities $A_{4p\to 4s}$ are tabulated.[15]

The production rate of reaction (13d) has the form:

$$\left(\frac{dN_{3p^54s}}{dt}\right)_{13d} = -\langle \sigma \cdot v \rangle_{3p^54s\to 3p^54p} N_{3p^54s} N_e \tag{15}$$

Because no satisfying value of the collision cross section has been found in the literature, it is evaluated at each iteration by solving in the homogeneous zone $\Sigma_{3p^54s\ \text{level}}\ \dot{\omega}_i = 0$. As the electron temperature is constant, the reaction rate constant is unchanged in the boundary layer.

The depopulation rate, due to resonant radiation, depends on the entire plasma. This feature is modeled by a schematic approach described below. The boundary layer is supposed to be stratified, i.e., without gradients parallel to the flat plate. By requiring radiative energy conservation on a slice having dy as a thickness, a relationship can be established between the number of photons emitted or absorbed by the slice and its variation of luminance, or similarly between the population balance and the luminance. Therefore, for each resonant level, we have to solve:

$$\frac{1}{N_{\text{res}}(\delta)}\left(\frac{dN_{\text{res}}}{dt}\right)_{\text{rad}} = -\frac{A_{r\to f}}{\sqrt{\pi}t(y)} \cdot \left(\int_0^y \frac{\partial m(y')}{\partial y} \beta[\tau(y) - \tau(y')]\, dy' - \int_y^\delta \frac{\partial m(y')}{\partial y} \beta[\tau(y') - \tau(y)]\, dy' + m(0)\beta[\tau(y)] + \beta[\tau(l) - \tau(y)] \right) \tag{16}$$

with:

l: homogeneous zone thickness

$A_{r\to f}$ = transition probability

$$t(y) = \frac{T(y)}{T(\delta)}$$

$$m(y) = \frac{N_{\text{res}}(y)}{N_{\text{res}}(\delta)}\, t(y)$$

$$\beta[\tau(y) - \tau(y')] = \frac{1}{4\pi k_0(y)\Delta\nu D(y)} \int_{\nu=0}^{\infty} \int_{\mu=1}^{0} \int_{\Phi=0}^{2\pi} \cdot e^{-\frac{\tau_\nu(y) - \tau_\nu(y')}{\mu}} k_\nu(y)\, d\nu\, d\mu\, d\Phi$$

$\Delta\nu D(y)$: broadening

$k_0(y)$: centerline absorption coefficient

$k_\nu(y)$ absorption coefficient

The β functions are calculated by neglecting the temperature and velocity gradients. The two resonant levels $^1p_1$ and $^3p_1$ must be considered separately.

1. $^3p_1$ Level

At the considered pressure (~120 Pa) all Lorentz broadening terms can be neglected compared to the Doppler one (due to thermal agitation). For k_ν a Doppler broadening profile is taken, which yields in the case of β:

$$\beta = \beta_0[k_0(y - y')] \tag{17}$$

with the β_0 function identical to Holstein's proposal.[16]

2. $^1p_1$ Level

For this level, the Lorentz broadening due to inelastic collisions (resonant broadening) cannot be neglected compared to the Doppler broadening. The Drawin[17] correction to β_0 is used.

IV. Numerical Estimation of Recombination Coefficient

The recombination of charged species is essentially accomplished through the direct recombination reaction:

$$Ar^+ + e^- + e^- \to Ar^* + e^- \tag{18a}$$

The global species conservation equation gives:

$$\sum_{i=1}^{p} \left(\frac{dN_i}{dt}\right) + \left(\frac{dN_{Ar^+}}{dt}\right) = 0 \tag{18b}$$

where p: number of excited levels.

The electroneutrality of the plasma can be expressed as:

$$\left(\frac{dN_{Ar^+}}{dt}\right) = \left(\frac{dN_e^-}{dt}\right) \tag{18c}$$

$$(18b) + (18c) \Rightarrow \left(\frac{dN_e^-}{dt}\right) = \sum_{i=1}^{p} \left(\frac{dN_i}{dt}\right) \tag{18d}$$

The relaxation time of excited levels with respect to the ground state being very short, it is correct to keep in the R.H.S. only dN_{fund}/dt. The fundamental level is preferably coupled with $3p^54s$ level:

$$\frac{dN_{\text{fund}}}{dt} = N_{3p^54s} N_e \langle \sigma \cdot v \rangle_{3p^54s\to f} - \left(\frac{dN_{\text{res}}}{dt}\right)_{\text{rad}} \tag{19a}$$

$$\Rightarrow \frac{dN_e}{dt} \sim \left(\frac{dN_{\text{res}}}{dt}\right)_{\text{rad}} - N_{3p^54s} N_e \langle \sigma \cdot v \rangle_{3p^54s\to f} \tag{19b}$$

Thus, at each iteration the comparison between the ion/electron recombination coefficient calculated with (19b) or (12b) can be carried out. We can notice that using (19b) or (12b) in the equation for the electron/ion pair is not important because the boundary layer is almost frozen for the charged particles.

V. Numerical Method

The system of equations that has been described above can be cast in the following form:

$$\rho u \frac{\partial \Phi}{\partial x} + \rho v \frac{\partial \Phi}{\partial y} = \frac{\partial}{\partial y}\left(\mathcal{D} \frac{\partial \Phi}{\partial y}\right) + S_\Phi \tag{20a}$$

with:

$$\Phi = (u, T, \alpha, Y_{3p^54s}) \tag{20b}$$

$$\mathcal{D} = \left(\mu, \frac{\lambda_{Ar^+} + \lambda_{Ar}}{C_p - r}, \rho D_{\text{amb}}, \rho D_m\right) \tag{20c}$$

The source terms are split as:

$$S_\Phi = \Phi S_{\Phi\text{lincar}} + S_{\Phi\text{n.lincar}} \tag{20d}$$

The detailed expressions of the linear and no-linear source terms follow:

$$S_{\Phi\text{lincar}} = \left(0, \frac{1}{C_p - r}\left(\frac{r}{\alpha} D_{\text{amb}} \frac{\partial \alpha}{\partial y} - \rho r \left(\frac{\partial u}{\partial x} + \frac{\partial v}{\partial y}\right)\right), 0, - \langle \sigma \cdot v \rangle_{3p^5 4s \to 3p^5 4p} \frac{N_e}{\rho}\right) \tag{21a}$$

$$S_{\Phi\text{n.lincar}} = \left(0, \frac{1}{C_p - r}\left(\frac{\rho}{\alpha} r D_{\text{amb}} \frac{\partial \alpha}{\partial y} \frac{\partial T}{\partial y} + E_i^0 \left(\frac{\partial}{\partial y}\left(\rho D_{\text{amb}} \frac{\partial \alpha}{\partial y}\right) + \dot{\omega}_{Ar^+}\right) + Q_{T-E}\right), \dot{\omega}_{Ar^+}, \dot{\omega}_{3p^5 4s(13a)} + \dot{\omega}_{3p^5 4s(13d)} + \dot{\omega}_{3p^5 4s(13h)}\right) \tag{21b}$$

Equation (20a) is solved with a modified version of the Patankar and Spalding method.[18] These parabolic equations are solved with an implicit space marching procedure. Two hundred points are used in the y-direction and ~3000 marching steps are needed in the x-direction (for 8.10^{-3} mm). Whenever it is possible, linearization is made for all equations in order to improve stability. Nevertheless, because of the stiffness of $3p^5 4s$ equation, its source terms cannot be linearized (except for the reaction 13d). This led us to use a rather small increment in the x-direction.

VI. Experiment

A. Flow Configuration and Boundary Conditions (Fig. 1)

The plasma source is a DC arcjet having the classical electrode configuration. The arc is initiated between the tip of a tungsten cathode and a nozzle-shaped copper anode. A power of 6 kW was applied to 9 l.mn^{-1} of argon. The freejet flows into a low-pressure test chamber (60 cm diameter) all maintained at the pressure 120 Pa. A stainless steel cooled plate is set along its flow direction. To avoid edge effects, this plate is larger than the spread of the jet (plate: 12 cm wide/15 cm long, jet: 10 cm diameter).

The freestream conditions are as follows: u_∞ = 680 m/s, T_∞ = 1500 K, T_e = 5500 K, P = 120 Pa, α_∞ = $1.358.10^{-2}$, $N_{3p^5 4s_\infty}$ = $3.1.10^{17}$ m^{-3}.

The wall boundary conditions are:

$$u_{\text{wall}} = 0 \text{ (no - slip boundary)} \tag{22a}$$

$$\left(\frac{\partial \alpha}{\partial y}\right)_{\text{wall}} = \left(\frac{1}{D_{\text{amb}}} \sqrt{\frac{kT_e}{m_{Ar}}}\, \alpha\right)_{\text{wall}} \tag{22b}$$

$$N_{3p^5 4s\text{wall}} = 0 \tag{22c}$$

$$T_{\text{wall}} = 400 \text{ K} \tag{22d}$$

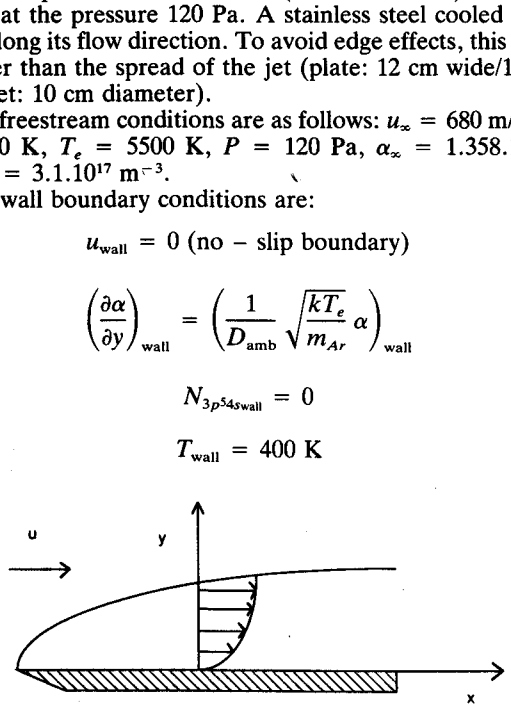

Fig. 1 Flow configuration.

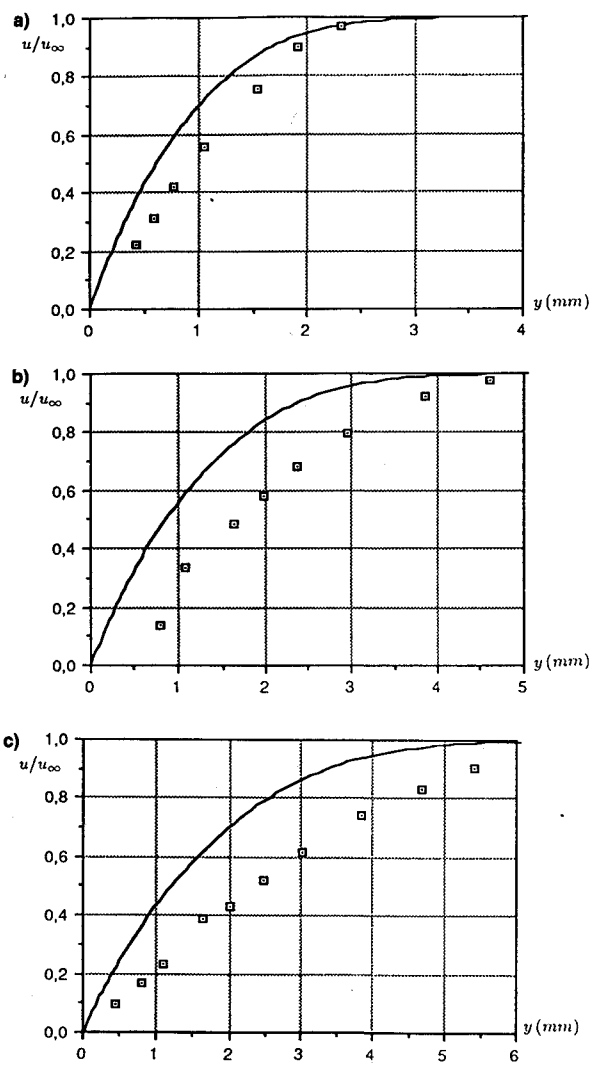

Fig. 2 Comparison of reduced profiles of velocity distribution at different x-locations: a) x = 2 mm; b) x = 4 mm; c) x = 8 mm.

B. Measurement Techniques

The measurements were made with an interferential Fabry Perot (FP) spectrometer. The spectrometer isolates a spectral band of $2.5.10^{-2}$ nm, which is sent in the FP (spectral resolution 10^{-3} nm). The measurement apparatus allows a spatial resolution of 0.3 mm crosswise and 0.5 mm streamwise. The population density of the metastable and resonant levels is determined by measuring the absorption coefficient profile of near I.R. (Infra Red) transitions of argon (transitions: 772.3 nm, 772.4 nm, 751.4 nm, 750 nm, which have respectively $^1p_1$, $^3p_1$, $^3p_2$, $^3p_0$ as lower levels). The atomic temperature is deduced from the effect of thermal broadening on this profile. The measurement of the intensity of the emission radiations gives the population of $3p^5 4p$, $3p^5 5p$, $3p^5 4d$ levels. Those levels verify the Saha equilibrium law and, thus, we can obtain electron density and temperature. The Doppler shift of the emission line of argon (following a direction making a small angle with xOy) gives the velocity (accuracy: 50 m/s). The population density of excited levels being small compared population density of the fundamental level, the pressure is obtained by the following relationship:

$$P = (N_{\text{fund}} + N_{\text{ions}})kT + N_e kT_e \tag{23}$$

VII. Results and Discussion

Figures 2–7 show the comparison of computations with experiments at different abscissa along the flat plate (x = 2,

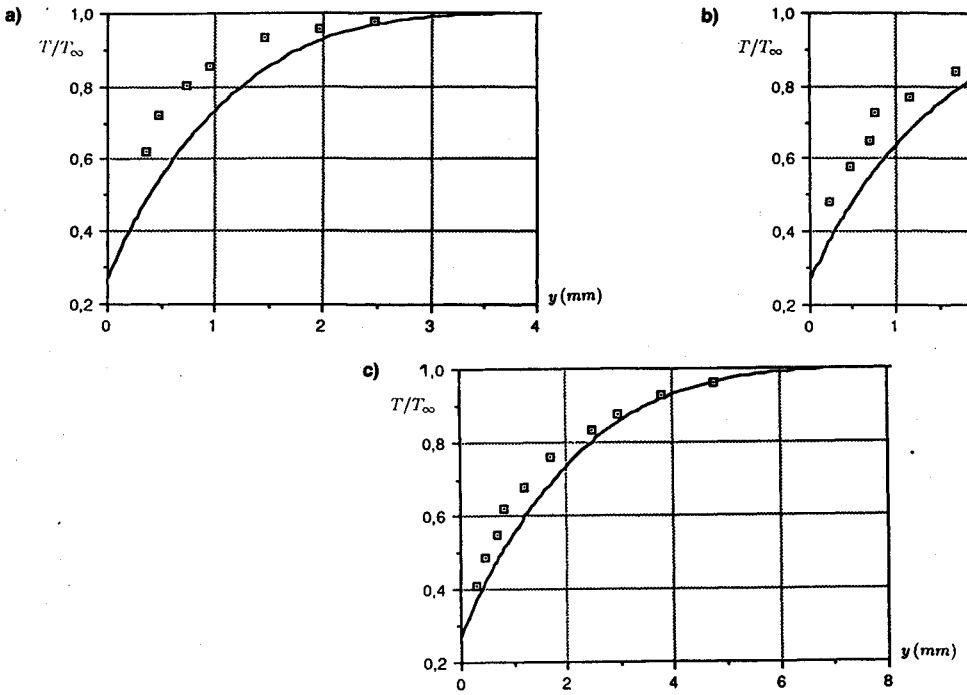

Fig. 3 Comparison of reduced profiles of temperature variations at different x-locations: a) $x = 2$ mm; b) $x = 4$ mm; c) $x = 8$ mm.

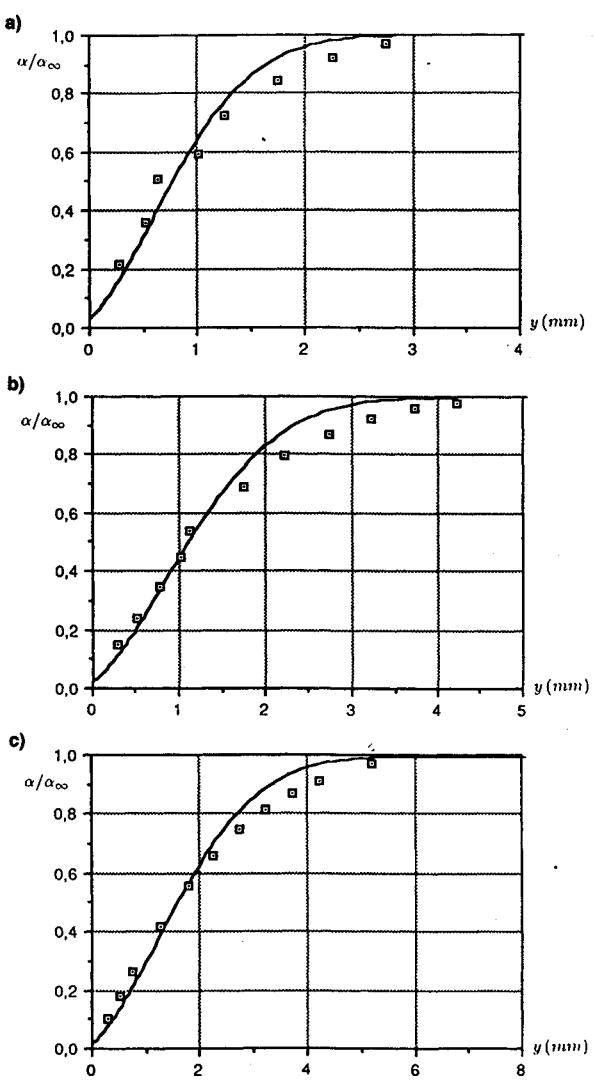

Fig. 4 Comparison of reduced profiles of ion mass fraction at different x-locations: a) $x = 2$ mm; b) $x = 4$ mm; c) $x = 8$ mm.

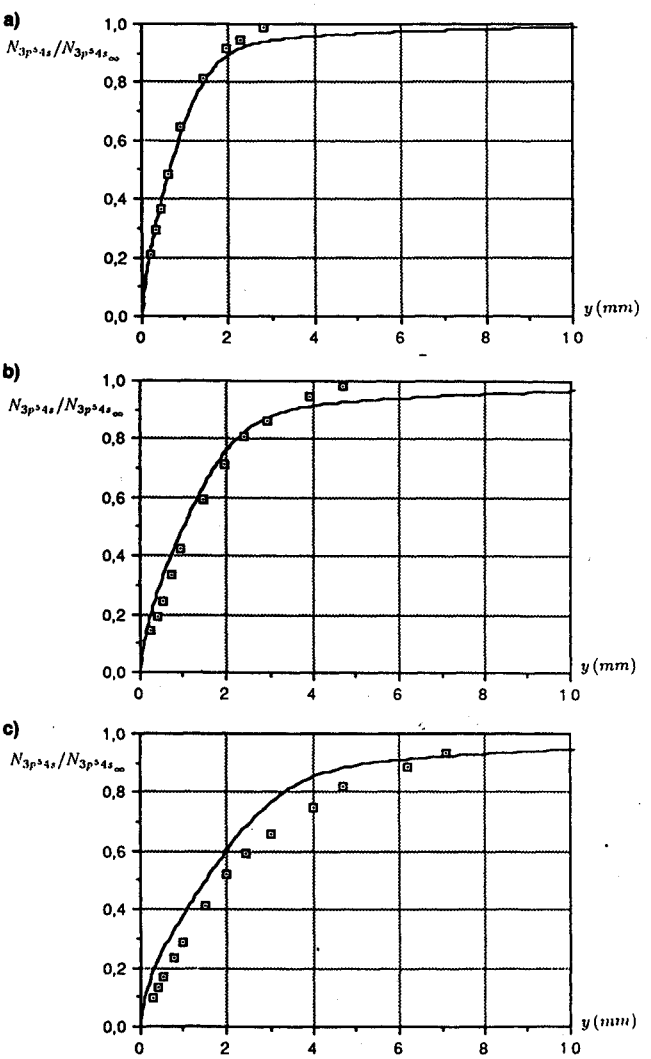

Fig. 5 Comparison of reduced profiles of population density of $3p^54s$ level at different x-locations: a) $x = 2$ mm; b) $x = 4$ mm; c) $x = 8$ mm.

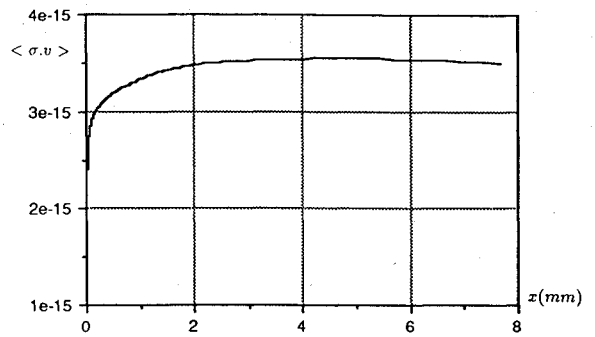

Fig. 6 Collision cross section $\langle \sigma \cdot v \rangle_{3p^54p \to 3p^54s}$ ($m^3 \cdot s^{-1}$) evolution along the plate.

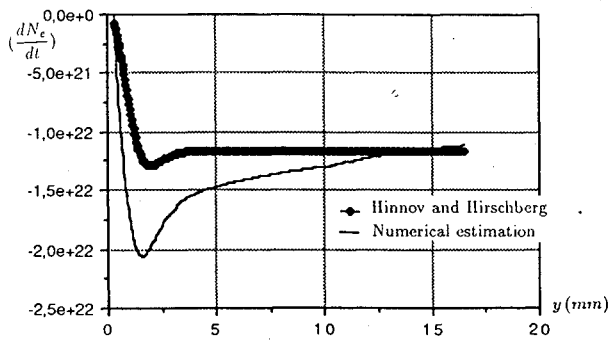

Fig. 7 Comparison of ion/electron recombination coefficient (part $\cdot m^{-3} \cdot s^{-1}$) at x = 2 mm.

4 and 8 mm). The overall agreement is fairly good, except a minor discrepancy on the velocity profiles (Figs. 2a–2c). This point is linked to the fact that velocity measurements are the less accurate, because obtained by small Doppler shift.

Figures 3a–3c provide a comparison of experimental and numerical results for atomic temperature. Except for the abscissa x = 2 mm where the validity of the boundary layer assumptions could be discussed, the numerical results remain in the experimental error margin (10%).

Figures 4a–4c show a very good agreement between experiments and numerics. We could note that the ion mass fraction evolution is principally determined by diffusion and convection contributions.

Agreement for the $3p^54s$ level (Figs. 5a–5c) is excellent. It was observed that accounting for the radiative transfer is absolutely necessary, especially in a boundary layer where emitting and absorbing zones are different, and also where the models using effective transition probabilities are not sufficient.

The collision cross section $\langle \sigma \cdot v \rangle_{3p^54s \to 3p^54p}$ that is calculated is consistent with a quasisteady behaviour along the flat plate (Fig. 6). The calculated value ($\sim 3.5 \times 10^{-15} m^3/s$) is one order of magnitude lower than the value proposed by Drawin.[19] Nevertheless, this result is in good agreement with the measurements of Copley and Lee,[20] they found $\langle \sigma \cdot v \rangle_{3p^54s \to 3p^54p} = 6.10^{-14}\ m^3 \cdot s^{-1}$ for kT_e = 3 eV, which is consistent with our value if an evolution with e^{kT_e} is assumed.

A comparison between the ion/electron recombination coefficient of Hinnov and Hirschberg[9] and the calculated one (Fig. 7) is made. Therefore, it can be observed that, when the radiative term becomes important compared to the collision term (which is true in our experiments), the local recombination coefficient will not depend only on local plasma values, but on the whole plasma through the resonant radiative transfer term. This effect, due to the radiative transfer, would be more significant in a supersonic or hypersonic flow where the Doppler displacement in the gradient zone makes the radiative transfer bigger.

VII. Conclusions

The velocity, heavy particle temperature, ion mass fraction, and population density of $3p^54s$ level of argon have been computed in a boundary layer. Analysis has been made in strong thermal nonequilibrium (atomic temperature 1500 K and electron temperature 5500 K). The calculated profiles compare fairly well with experiments.

A kinetic model describing the evolution of the $3p^54s$ level has been developed with the assumption of a strong coupling between the metastable and resonant levels, which allows use of a global conservation equation. The significant role of radiative transfer has been pointed out. Its influence on the ion/electron recombination rate has also been exhibited, leading to a strong difference between the value obtained from Hinnov and Hirschberg[9] and the calculated one.

Further research is required to improve the modeling of the transport coefficients in order to avoid the use of empirical laws. However, this numerical approach of a flowing plasma is very promising and will be applied to more complex plasmas such as nitrogen or air plasmas.

References

[1]Matsuoka, K., and Nishida, M., "Non Equilibrium Stagnation Point Boundary Layer of a Partially Ionized Gas," Department of Aeronautical Engineering Kyoto University, Current Papers, CP.30, May 1971.

[2]Hirschfelder, J. O., Curtiss, C. F., and Bird, R. B., *Molecular Theory of Gases and Liquids*, John Wiley, New York, 1954.

[3]Devoto, R. S., "Transport Coefficients of Partially Ionized Argon," *Physics of Fluids*, Vol. 10, No. 2, 1967, pp. 354–364.

[4]Ellis, E., and Twiddy, N. D., "Time-resolved Optical Absorption Measurements of Excited Atom Concentrations in Argon After-glow," *Journal of Physics B*, Vol. 2, No. 12, 1969, pp. 1366–1377.

[5]Kharrazi, S., "Contribution à l'étude expérimentale des processus régissant l'évolution des espèces présentes au sein d'un milieu ionisé par la technique de post-décharge," *Thesis—University of Grenoble* (France), 1974.

[6]Bochkova, O. P., Sukiasyan, E. A., and Tolmachev, Y., "Decay of Metastable Argon Atoms by Thermal Electrons," Optikai Spektroskopia (Optics and Spectroscopy), Vol. 38, No. 1, 1975, pp. 104–105.

[7]Jaffrin, H. J., "Shock Structure in a Partially Ionized Gas," *Physics of Fluids*, Vol. 8, No. 4, 1965, pp. 606–625.

[8]Knöös, S., "Boundary Layer Structure in a Shock Generated Plasma," *Journal of Plasma Physics*, Vol. 2, Part 2, June 1968, pp. 207–242.

[9]Hinnov, E., and Hirschberg, J. G., "Electron-Ion Recombination in Dense Plasma," *Physical Review*, Vol. 125, 1962, pp. 795–801.

[10]Vervisch, P., "Etude de la cinétique d'un plasma d'argon basse pression au voisinage d'une paroi," *Thesis—University of Rowen* (France), 1978.

[11]Vervisch, P., Terrier, M., and Valentin, P., "Etude de la cinétique du niveau $3p^54s$ dans une couche limite de plasma d'argon basse pression," *Journal de Physique*, t. 38, juil. 1977, pp. 783–787.

[12]Lloyd, Teubner, P. J., Weigold, E., and Hood, S. T., "Excitation of the First Excited State in Argon by Electron Bombardment," *Journal of Physics B: Atomic and Molecular Physics*, Vol. 5, No. 2, 1972, pp. 44–47 and "Excitation Functions for the Formation of Metastable He and Ar by Electron Impact," *Journal of Physics B: Atomic and Molecular Physics*, Vol. 5, No. 9, 1972, pp. 1712–1718.

[13]Borst, W. L., "Excitation of Metastable Argon and Helium Atoms by Electron Impact," *Physical Review A: General Physics*, Vol. 9, No. 3, 1974, pp. 1195–2000.

[14]Brunt, King, and Read, "A Study of Resonance Structure in Neon, Argon, Krypton and Xenon using Metastable Excitation by Electron Impact with High Energy Resolution," *Journal of Physics B: Atomic and Molecular Physics*, Vol. 9, No. 13, 1976, pp. 2195–2207.

[15]Wiese, W. L., Smith, M. W., and Miles, P. M. "Atomic Transition Probabilities," NFRDS-NBS, No. 22, Vol. 2, Oct. 69, Library of Congress Catalog Card No. 65-60078.

[16]Holstein, T., "Imprisonment of Resonance Radiation in Gases," *Physical Review*, Vol. 83, 1951, pp. 1159–1168.

[17]Drawin, H. W., and Emard, F., "Optical Escape Factors for

Bound-bound and Free-bound Radiation from Plasma Constant Source Function," *Beiträge aus der Plasmaphysik*, Vol. 13, No. 3, 1973, pp. 143–168.

[18]Vandromme, D., "Turbulence Modelling in Variable Density Flow," Ph.D. Thesis, Von Karman Instute, June 1980.

[19]Drawin, H. W., "Influence of Atom-Atom Collisions on the Collisional-radiative Ionization and Recombination Coefficients of Hydrogen Plasmas," *Zeitschrift für Physik*, Vol. 225, No. 5, 1969, pp. 483–493.

[20]Copley, G. H., and Lee, C. S., "Electron Excitation and Deexcitation Coefficients for the $^3p_2$, $^3p_1$, $^3p_0$, and $^1p_1$ Levels of Argon," *Canadian Journal of Physics*, Vol. 53, No. 18, 1975, pp. 1705–1714.